Single-Atom Lithiophilic Sites Confined within Ordered Porous Carbon for Ultrastable Lithium Metal Anodes

Wenzhong Huang, Shanlin Liu, Ruohan Yu, Liang Zhou [ID]*, Zhenhui Liu*, and Liqiang Mai** [ID]

Attributing to the high specific capacity and low electrochemical reduction potential, lithium (Li) metal is regarded as the most promising anode for high-energy Li batteries. However, the growth of lithium dendrites and huge volume change seriously limit the development of lithium metal batteries. To overcome these challenges, an ordered mesoporous N-doped carbon with lithiophilic single atoms is proposed to induce uniform nucleation and deposition of Li metal. Benefiting from the synergistic effects of interconnected three-dimensional ordered mesoporous structures and abundant lithiophilic single-atom sites, regulated local current density and rapid mass transfer can be achieved, leading to the uniform Li deposition with inhibition of dendrites and buffered volume expansion. As a result, the as-fabricated anode exhibits a high CE of 99.8% for 200 cycles. A stable voltage hysteresis of 14 mV at 5 mA cm^{-2} could be maintained for more than 1330 h in the symmetric cell. Furthermore, the full cell coupled with commercial LiFePO$_4$ exhibits high reversible capacity of 108 mAh g^{-1} and average Coulombic efficiency of 99.8% from 5th to 350th cycles at 1 C. The ordered mesoporous carbon host with abundant lithiophilic single-atom sites delivers new inspirations into rational design of high-performance Li metal anodes.

1. Introduction

Compared with commercial lithium-ion battery anode materials, lithium (Li) metal possesses ultrahigh theoretical specific capacity (3860 mAh g^{-1}), the lowest potential (-3.040 V vs standard hydrogen electrode, SHE), as well as good electrical conductivity.[1,2] Therefore, applying Li meal as the anode can greatly increase the energy density of the battery and accelerate the development of advanced batteries.[3] For instance, the energy density of batteries based on Li metal is higher than that based on commercial graphite anode for more than 1.5 times, and also higher than that based on Si anode for nearly 100 Wh kg^{-1}.[4] In addition, when coupled with an ideal cathode material (such as sulfur or oxygen), the full cells can achieve high theoretical energy density (Li-S batteries: 2600 Wh kg^{-1}, Li-O$_2$ batteries: 11 400 Wh kg^{-1}), which are almost comparable to the energy density of petroleum (13 200 Wh kg^{-1}).[5–7] Therefore, researches on Li metal anode are of great significance to achieve new breakthroughs in secondary batteries.

Despite years of researches, the Li metal anode still faces safety and capacity issues caused by the lithium dendrites growth and huge volume change. To solve these problems, numerous efforts have been devoted, including electrolyte additives,[8,9] modified electrodes,[10,11] artificial SEI layers,[12,13] as well as solid electrolytes,[14–17] etc. Among these studies, rational design of Li host material has been regarded as a promising strategy, which can regulate local current density, homogenize Li$^+$ flux and provide sufficient space for Li accommodation. As one of the potential candidates for Li host, carbon materials draw lots of attention by advantages of high electrical conductivity, good electrochemical stability, and low mass density.[18–20] However, the lithiophobic property of carbon-based materials has become an important bottleneck, hindering their application as lithium metal host.[21]

Recently, the introduction of metal single atom to form M-N-C sites (M, N, C refer to metal, nitrogen, and carbon atoms, respectively) has emerged as an effective choice.[22,23] Due to the strong Li adsorption energy and low cost, Ni-N-C active sites have drawn increasing attentions.[24] However, maintaining the stability of metal single atoms is a key problem owing to their trend to agglomerate, so it is of a great importance to choose suitable supports to construct stable coordination structure.[25] Among various supports, N-doped three-dimensional (3D) ordered mesoporous carbon with uniform mesopores and abundant N doping has showed great potential, which can provide adequate surface areas and anchored sites to stabilize metal single atoms. Besides, the interconnected ordered mesoporous channels and large specific surface areas can enhanced transport pathway for electrons and Li ions, which facilitate a

W. Huang, S. Liu, Prof. L. Zhou, L. Mai
State Key Laboratory of Advanced Technology for Materials Synthesis and Processing, Wuhan University of Technology, Wuhan 430070, China
E-mail: mlq518@whut.edu.cn
R. Yu
Nanostructure Research Centre, Wuhan University of Technology, Wuhan 430070, China
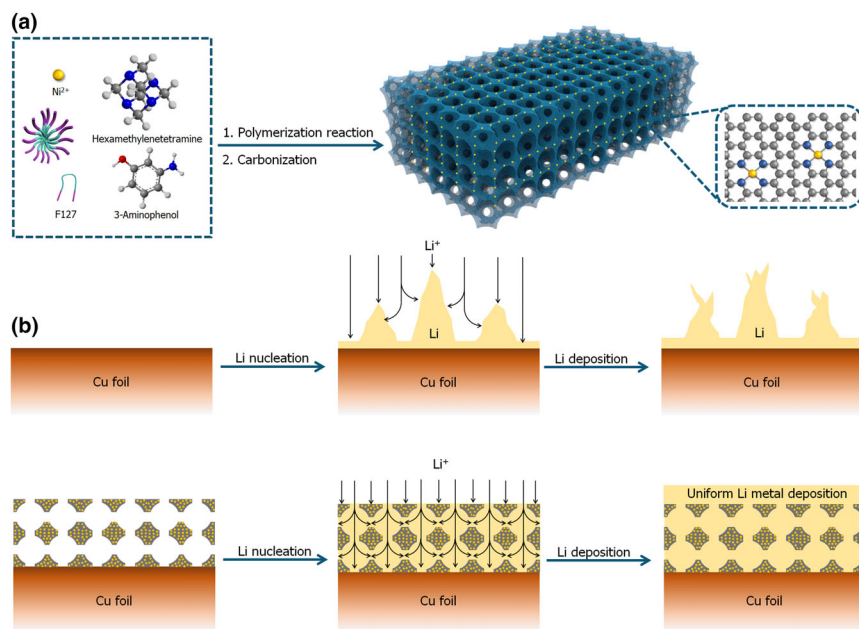Dr. Z. Liu
College of Material Science and Engineering, Nanjing University of Aeronautics and Astronautics, Nanjing 210016, China
E-mail: lzh0328@nuaa.edu.cn
L. Mai
Foshan Xianhu Laboratory of the Advanced Energy Science and Technology Guangdong Laboratory, Xianhu hydrogen Valley, Foshan 528200, China
E-mail: mlq518@whut.edu.cn
[ID] The ORCID identification number(s) for the author(s) of this article can be found under https://doi.org/10.1002/eem2.12466.

Figure 1. a) Schematics of NOMC-Ni synthesis; b) schematic illustration of Li nucleation and deposition process on Cu foil (top) and NOMC-Ni-coated Cu foil (bottom).

uniform charge distribution and a regulated Li^+ flux dispersion on the electrode, suppressing the unfavorable side reactions between Li and electrolyte and promoting the dendrite-free deposition of Li.[21,26] The mesoporous structures also buffer the infinite volume change during Li plating/stripping, which is beneficial to build a robust solid electrolyte interface (SEI) layer.[27]

Herein, we design an N-doped ordered mesoporous carbon with interconnected 3D mesopore channels and abundant uniform dispersed lithiophilic single-atom sites (NOMC-Ni), which possesses both advantages of atomic Ni lithiophilic site and 3D ordered mesopore structures on the optimization of Li metal anode. As shown in **Figure 1**, the NOMC-Ni can effectively promote the uniform deposition of Li metal in the ordered mesopore channels and effectively suppress the growth of Li dendrites. Benefiting from the synergistic effects of the 3D-ordered mesoporous structure and lithiophilic single atoms, when applied as a Li metal host, NOMC-Ni/Li electrode exhibits a high CE of 99.8% after 200 cycles and extremely low nucleation overpotential (~31 mV). Besides, when coupled with commercial $LiFePO_4$ (LFP), the Li-NOMC-Ni‖LFP exhibits high capacity of 108 mAh g^{-1} and average Coulombic efficiency (CE) up to 99.8% during cycles from 5th to 350th at 1 C.

2. Results and Discussion

2.1. Synthesis and Material Characteristics

The synthetic process of NOMC-Ni is shown in Figure 1a. First, 3-aminophenol/formaldehyde/F127 was fabricated via a soft-templating method. Afterward, the 3-aminophenol/formaldehyde/F127 composite was mixed with $NiCl_2$ and the Ni^{2+} ions can be complexed by N-containing organic groups. After carbonization, F127 templates were removed while the polymer of 3-aminophenol/formaldehyde/F127 was transformed into N-doped carbon with the formation of Ni-N-C sites. In addition, ordered mesoporous carbon (OMC) without N-dopant was also synthesized for comparison. Figure 1b presents the schematic comparison of Li ion nucleation and deposition on Cu foil and NOMC-Ni. The unordered Li deposition happens on Cu surface owing to the nonuniform electron density attributed to the rough Cu surface, which might lead to the formation of Li dendrites and "dead Li". By contrast, ascribing to the lithiophilic mesostructure, when NOMC-Ni was coated on Cu foil, the Li^+ prefers to fill in the ordered mesoporous and form uniform Li metal layer, thus enhancing the cycling stability.

As depicted in Figures S1–S11, Supporting Information, X-ray diffraction (XRD) patterns of the samples show broad diffraction peaks at $\sim25^o$ and $\sim45^o$, which are characteristic for amorphous carbon. These weak and broad peaks indicate that the low crystalline of the carbonization products.[28] Small-angle X-ray diffraction (SAXD) pattern of the NOMC-Ni shows three weak peaks, which could be indexed to the (110), (200), and (211) reflections of the body-centered cubic $Im\overline{3}m$ symmetry, suggesting a highly ordered cubic mesostructure is obtained (**Figure 2a**).[29] NOMC shows a similar mesoporous structure with NOMC-Ni, which indicates that the introduction of single Ni atoms does not influence the mesostructure of NOMC (Figure 1a). OMC and NOMC were prepared through adopting different precursors, leading to the differences in the cell parameters of their ordered mesoporous structures. According to the reports on ordered mesoporous carbon materials, NOMC possess larger interplanar spacing in (110) face than that of OMC.[29,30]

Fourier-transformed infrared (FT-IR) spectra were conducted to investigate the transformation of structures. As for the 3-aminophenol/formaldehyde/F127 composite, it can be observed that the broad band at 3425 cm^{-1} is ascribed to the vibration of hydroxyl group (−OH), while the band at 2910 cm^{-1} is attributed to CH_2 asymmetric stretching.[31] In addition, the bands at 1628 cm^{-1} and 1452 cm^{-1} are corresponded to amines (NH_2) and C-H stretching, respectively.[31] After carbonization, the peaks of functional groups of ordered mesoporous carbon disappear, indicating 3-aminophenol/formaldehyde/F127 polymer has been transformed into amorphous carbon (Figure S2, Supporting Information). Besides, the graphitization degree of samples could be confirmed by the Raman spectra (Figure S3, Supporting Information). The I_D/I_G of NOMC-Ni, NMOC, and OMC are 0.98, 0.96, and 0.92, respectively, indicating that all the samples still possess a degree of graphitization.

To study the coordination structure, Fourier-transformed extended X-ray absorption fine structure (EXAFS) spectra in the R space spectra were collected. As shown in Figure 2b, no peaks for Ni–Ni bond could be observed in the NOMC-Ni sample, indicating that there are no Ni clusters and nanoparticles exist in NOMC-Ni. The main existence forms of Ni species are atomic Ni-N-C sites. X-ray photoelectron spectroscopy (XPS) of NOMC-Ni was also carried out to study the chemical composition and elemental states. The XPS survey confirms

the existence of C, O, and N (Figure S4, Supporting Information). Due to the extremely low Ni content (~0.074 wt.%, data collected from inductively coupled plasma optical emission spectroscopy), no significant Ni peak could be detected (Figure S5, Supporting Information). The high-resolution XPS spectrum of N 1 s is shown in Figure 2c. The N 1 s peaks could be deconvoluted into oxidized N species (~404.8 eV), quaternary (~401.9 eV), pyrrolic (~400.9 eV), Ni-N (~398.8 eV), and pyridinic (~398.0 eV), respectively.[23] The existence of Ni-N confirms the strong interaction between the single

Ni atoms and N atoms from carbon host. In addition, nitrogen adsorption–desorption isotherms further verify the high porosity of the NOMC-Ni. The specific surface areas of NOMC-Ni are 489.51 $m^2 \, g^{-1}$, and the pore dimension mainly distributes between 4 and 5 nm (Figure S6, Supporting Information). The large specific surface and uniform mesoporous distribution are helpful for the uniform Li deposition.

Scanning electron microscopy (SEM) and transmission electron microscopy (TEM) were applied to identify the morphology of different
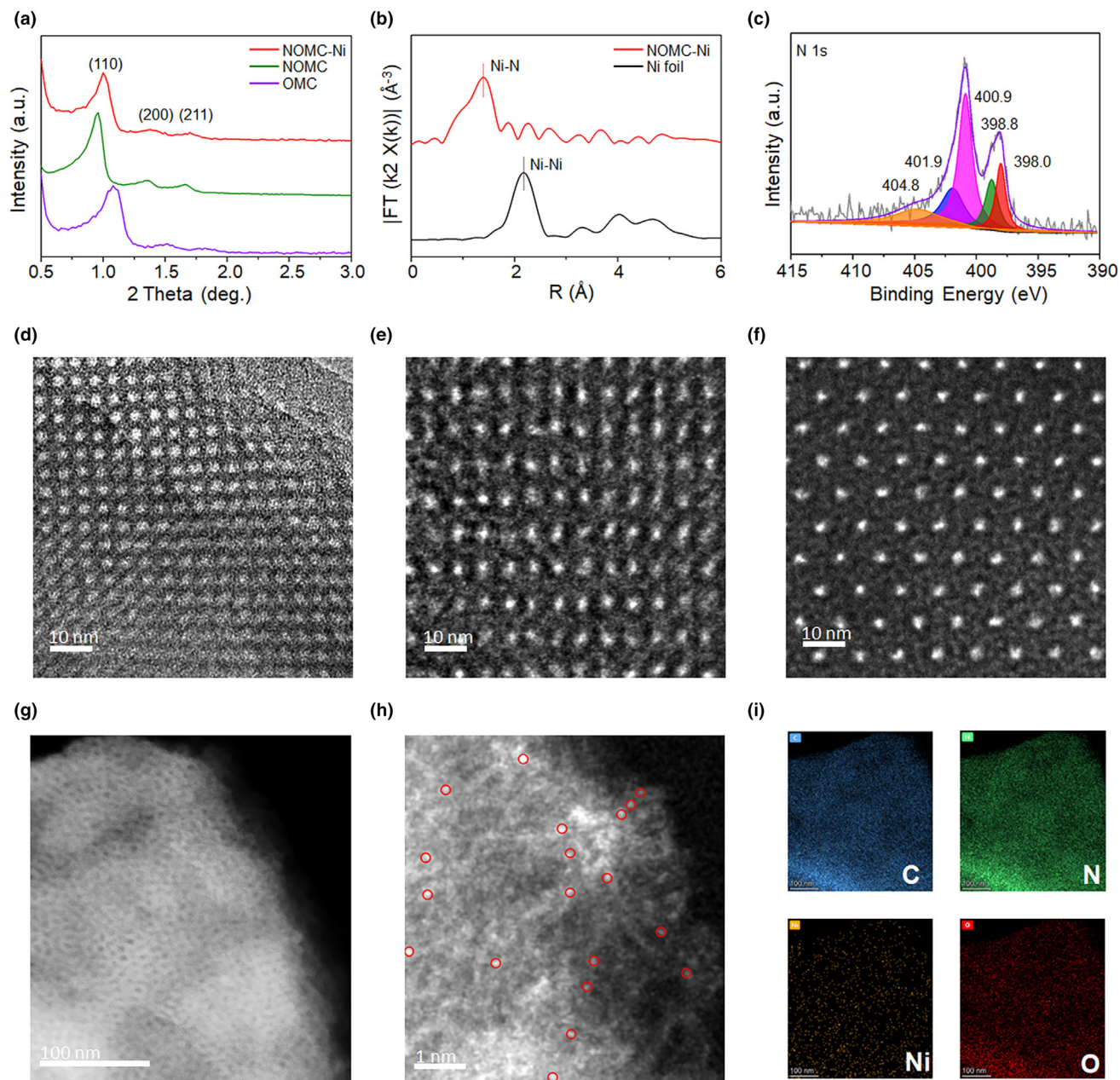

Figure 2. a) SAXD patterns of NOMC-Ni, NOMC, and OMC. b) Fourier-transformed EXAFS spectra of NOMC-Ni and the Ni foil. c) N 1 s XPS spectrum of NOMC-Ni; TEM images of NOMC-Ni viewed along d) (100), e) (110) and f) (111) directions. g) TEM image, h) HAADF-STEM image, and i) EDX elemental maps of NOMC-Ni (scale bar dimensions in i) are all 100 nm).

samples. According to Figure S7, Supporting Information, it can be observed that the morphologies of all the three samples are irregular micron-sized particles.[29] TEM images of NOMC-Ni were also provided. Figure 2d–f present NOMC-Ni viewed along (100), (110), and (111) directions, further confirm the cubic ordered mesoporous structure. As depicted in Figure 2g, uniform-dispersed Ni single atoms can be found (light spots). Besides, the high-angle annular dark field scanning transmission electron microscopy (HAADF-STEM, Figure 2h) and energy-dispersive X-ray (EDX) test, Figure 2i displays a uniform distribution of C, N, Ni, and O.

To study the Li deposition behavior, ex situ SEM images of different electrodes prepared with a current density of 1 mA cm^{-2} after 1 and 2 h were provided (**Figure 3**). When compared with Cu electrode (Figure 3a,b), it can be noticed that mesoporous materials can effectively alleviate the growth of Li dendrites. After the introduction of N, the growth of dendrites will be slightly mitigated (Figure 3c,f). In these mesoporous carbon materials, it is worth mentioning that NOMC-Ni can maintain a smooth surface even after 2 h of deposition. The smooth surface of NOMCE-Ni indicates that owing to the rich mesoporous and introduction of Ni single atoms, the fabricated electrode can effectively inhibit the growth of Li dendrites during cycling and lead to uniform Li nucleation and deposition (Figure 3g,h). In addition, the cross-sectional SEM of Cu and NOMC-Ni before/after 2 h Li deposition at 1 mA cm^{-2} has also been carried out to study the volume change during test (Figure 3i–l). As expected, massive Li dendrites can be observed on the Cu electrode while the thickness of NOMC-Ni electrode just increases from 31 to 32 {m without formation of Li dendrites. These results indicate that the NOMC-Ni host can effectively inhibit the growth of Li dendrite and buffer the volume expansion.

2.2. Electrochemical Performances

As a key parameter to reflect the loos Li$^+$ during each cycle and predict cycling stability of Li metal battery, CEs of different working electrodes cycled at different current densities with an areal capacity of 1 mAh cm^{-2} are provided (**Figure 4**a–b, Figures S8 and S9, Supporting Information).[32] As shown in Figure 4a, the CE of NOMC-Ni increases from 88.4% for the first cycle to 97.7% for the 11th cycle. In addition, a high CE of 99.8% could be achieved after 200 cycles at 0.5 mA cm^{-2}. However, for NOMC electrode, the CE reaches 86.4% at the 20th cycle and it begins to decay after 30 cycles. Besides, the CE of OMC decreases to 61.5% at 82th cycles. The CE of bare Cu stabilizes at 84.3% after 15 cycles, revealing limited cycling life. Li plating/stripping profiles at the 80th cycle of different electrodes are also displayed (Figure S8, Supporting Information). The NOMC-Ni electrode shows a flat and smooth voltage curve, with a nucleation overpotential of about 31 mV, which is much lower than those of Cu (98 mV), OMC (80 mV), and NOMC (102 mV) electrodes, confirming stable lithium stripping/plating and fast lithium migration kinetics. When the current density is increased to 1 mA cm^{-2}, NOMC-Ni also performs the best cycling property with a high average CE of 97.3% from 5th to 150th cycles and lowest voltage hysteresis of 15 mV among all electrodes (Figure 4b, Figure S9, Supporting Information), demonstrating the obvious advantages of NOMC-Ni as Li host. Besides, when compared with Cu electrodes, the slopes in the charge–discharge curves of NOMC-Ni/Li electrodes can be attributed to the intercalation/deintercalation of Li$^+$ into/from the NOMC-Ni.[33–36]

The Li stripping/plating performances of Cu, OMC, NOMC, and NOMC-Ni in symmetrical cells were also studied. As depicted in
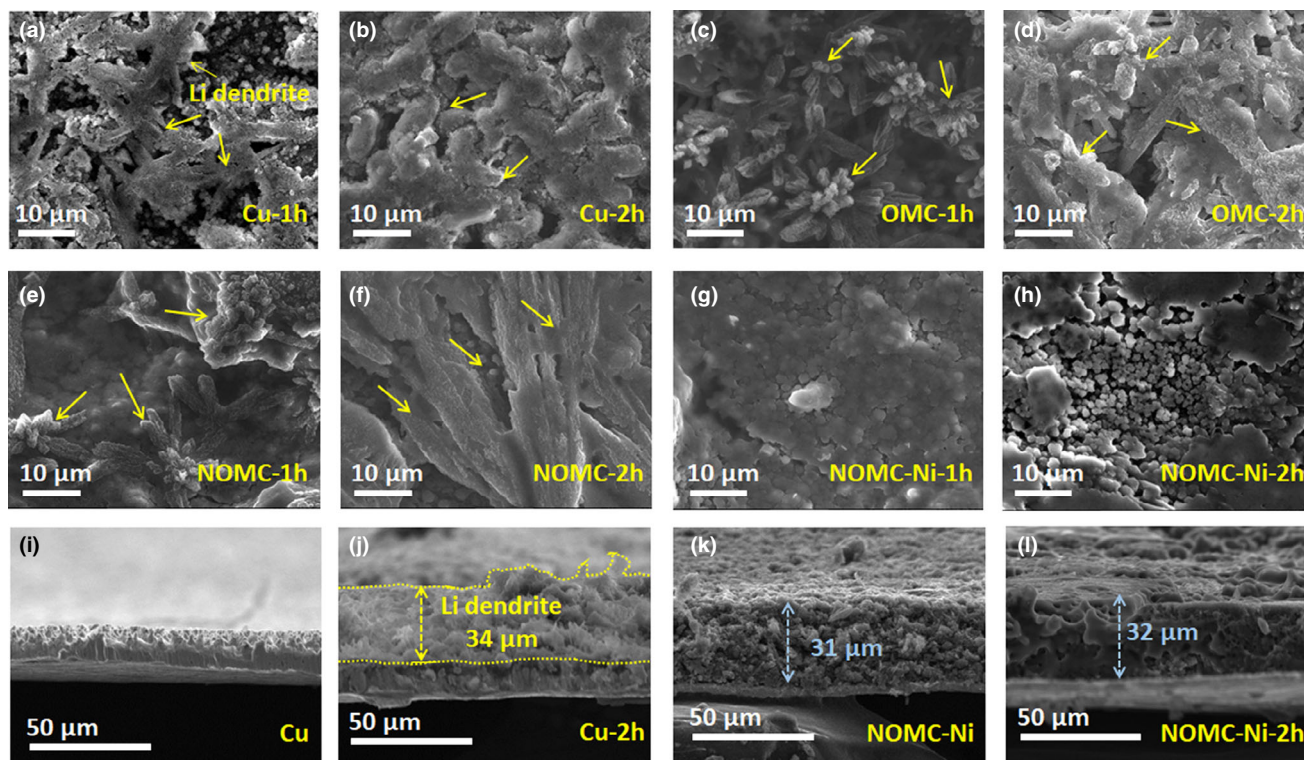

Figure 3. SEM images of Li deposition at 1 mA cm^{-2} on a, b) Cu electrode, c, d) OMC electrode, e, f) NOMC electrode and g, h) NOMC-Ni electrode for 1 and 2 h, respectively. Cross-sectional SEM of i, j) Cu electrode and k, l) NOMC-Ni electrode before and after 2 h Li deposition at 1 mA cm^{-2}.
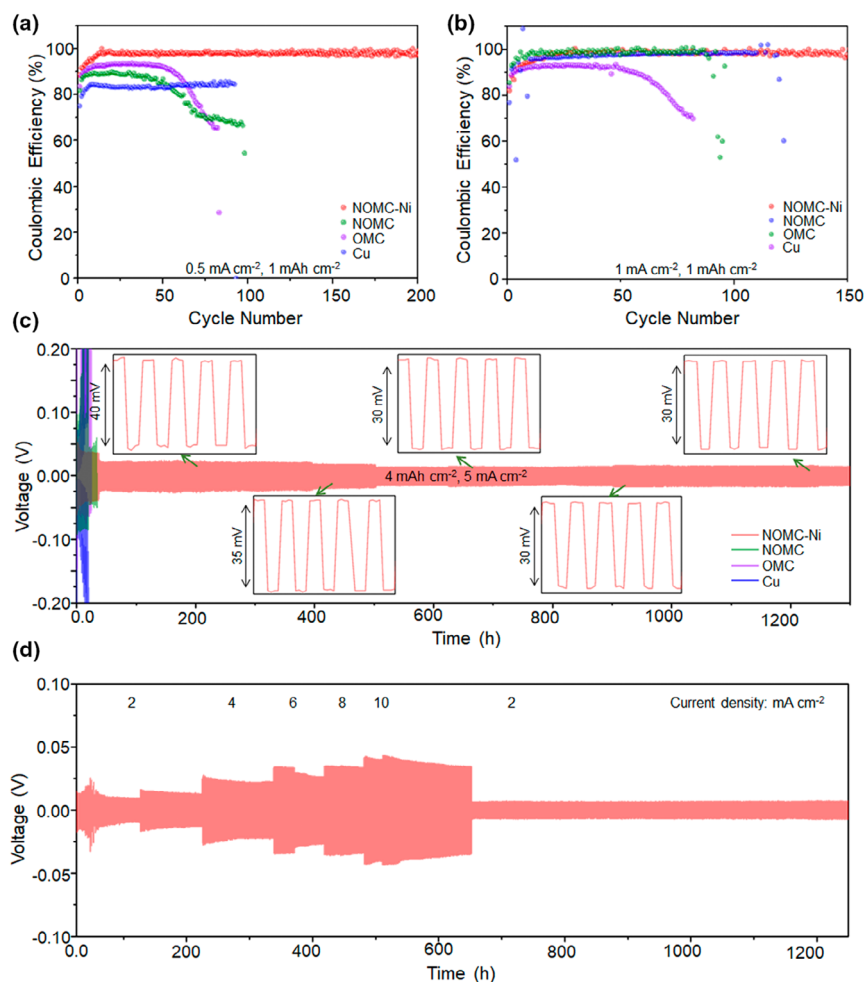
4 of 7

Figure 4. Electrochemical performance of Cu, OMC, NOMC, and NOMC-Ni: CEs at current densities of a) 0.5 mA cm^{-2} and b) 1 mA cm^{-2} for a total Li deposition capacity of 1 mA h cm^{-2}. c) Cycling performance of these electrodes in symmetric cells with Li plating/stripping for 4 mAh cm^{-2} at a current density of 5 mA cm^{-2}. d) Rate performance of NOMC-Ni cells obtained at different current densities of 2, 4, 6, 8, and 10 mA cm^{-2} with a Li deposition capacity of 1 mA h cm^{-2}.

formation of stable interface and voltage polarizations.[25,31,37] When current density is returned to 2 mA cm^{-2}, the voltage hysteresis can return to the original value, confirming the excellent stability of Li metal anode with NOMC-Ni as the host.

NOMC-Ni/Li||LFP full cell was assembled to evaluate the potential practical application of NOMC-Ni. As depicted in **Figure 5**a,b, the NOMC-Ni/Li||LFP shows excellent rate performance at C-rates from 0.2 to 2 C. The specific capacities at 0.2, 0.5, 1, and 2 C are 161, 151, 141, and 130 mAh g^{-1}, respectively. More importantly, the full cell also exhibits relatively high capacity of 115 mAh g^{-1} after 230 cycles at 0.5 C with 99.1% CE. The full cell could also maintain 108 mAh g^{-1} after 350 cycles at 1 C with 99.8% CE. Besides, the cycling performance of Cu/Li have also been tested for comparison. As shown in Figure S10, Supporting Information, the capacity of Cu/Li decay to 0 rapidly within 20th cycles at 0.5 and 1 C, confirming the poor cycling performance which can be attributed to the uneven deposition of lithium metal and growth of Li, which is consistent to the results of ex situ SEM (Figure 3i–j). On the contrary, the excellent cycling performance of NOMC-Ni/Li||LFP indicates that the NOMC-Ni/Li anode possesses excellent stability, which is attributed to inhibiting effects of NOMC-Ni host on the growth of lithium dendrites.

In addition, the electrochemical performances of LFP were also presented as comparison. When charging/discharging from 0.2 to 1 C, the discharge specific capacities of Li||LFP half-cell are 164.5, 160.5, 154.5 mAh g^{-1}, respectively (Figure S11a,b, Supporting Information). Even though the discharge specific capacity is relatively high, the cycling performances of Li||LFP at 0.5 and 1 C are very poor (Figure S11c,d, Supporting Information). The half-cell could only maintain 82.3% CE after 200 cycles at 0.5 C with capacity of 130 mAh g^{-1}. Besides, when tested under 1 C, the CE drops from 99.7% to 30.1% after 80 cycles with only 92.8 mAh g^{-1} capacity maintained. The poor cycling performance of Li||LFP also indicates the positive impact of NOMC-Ni as the host for Li metal anode.

3. Conclusion

In summary, a facile strategy has been proposed to prepare the N-doped ordered mesoporous carbon loaded with single-atom lithiophilic sites as an ideal host for ultrastable lithium metal anode. Benefiting from the uniform dispersed lithiophlilic Ni-N-C sites and the 3D interconnected ordered mesoporous structure, the Li metal could deposit uniformly on the NOMC-Ni with suppressed Li dendrite growth. Excellent cycling performance with low hysteresis voltage in symmetric
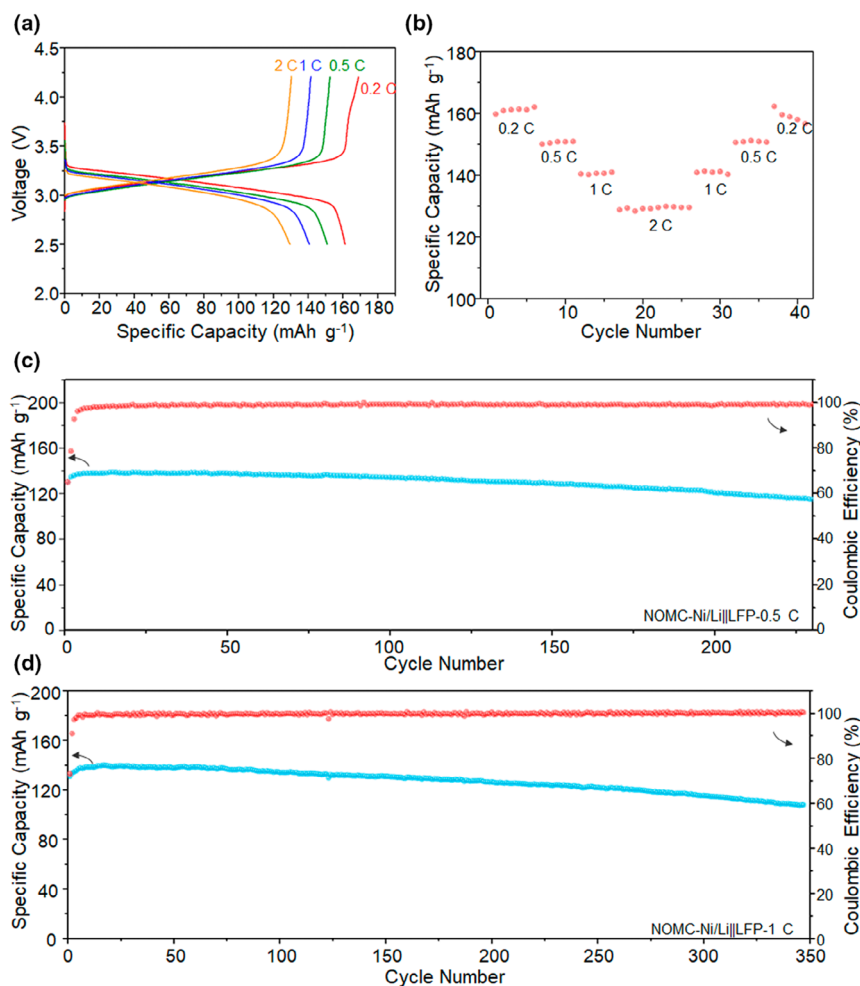
Figure 4c, the NOMC-Ni symmetric cell exhibits stable voltage curves with a voltage hysteresis of 14 mV and ultralong cycling life for more than 1330 h at 5 mA cm^{-2}. In contrast, the NOMC symmetric cell shows large fluctuation after cycling for 32 h, which is attributed to the SEI accumulation and the growth of Li dendrite. Without the positive effects of Ni single atoms, symmetric cells adopting Cu and OMC as lithium metal host could not maintain stable hysteresis voltage after 20 h. The insert pattern shows the enlargement of voltage curves at different cycles. When compared with other cells, the smoother and flatter voltage profiles of NOMC-Ni confirm the contributions of ordered mesoporous structure and atomic Ni doping to low local current density and fast electron transport, resulting in uniform Li stripping/plating. Rate capability of NOMC-Ni was also characterized by assembling symmetric cell and testing at current densities from 2 to 10 mA cm^{-2} at a high areal capacity (4 mAh cm^{-2}). As shown in Figure 4d, the voltage hysteresis of 15, 25, 30, 34, and 41 mV are obtained at current densities of 2, 4, 6, 8, and 10 mA cm^{-2}. During the test, the small fluctuation of the curves might be caused by the

Figure 5. a) Charge/discharge curves and b) rate capability of NOMC-Ni/Li‖LFP full cells at different rates from 0.2 to 2 C. Cycling stability of full cells at c) 0.5 C and d) 1 C.

cell could be realized. The full cell assembled with LFP also shows enhanced cycling stability. The combination of the single atomic metal lithiophilic sites and 3D-ordered mesopore structures sheds new light on the design of stable Li metal anodes and provides an opportunity for the development of ultrastable Li metal battery systems.

4. Experimental Section

Detailed information related to the synthesis of active electrodes, physicochemical characterization, and electrochemical evaluation of bifunctional electrodes towards UOR and supercapacitor application is provided in Supporting Information.

Conflict of interest

The authors declare that they have no conflict of interest.

Supporting Information

Supporting Information is available from the Wiley Online Library or from the author.

[1] B. Liu, J.-G. Zhang, W. Xu, *Joule* **2018**, *2*, 833.
[2] X. Shen, H. Liu, X.-B. Cheng, C. Yan, J.-Q. Huang, *Energy Stor. Mater.* **2018**, *12*, 161.
[3] J. Guo, H. Pei, Y. Dou, S. Zhao, G. Shao, J. Liu, *Adv. Funct. Mater.* **2021**, *31*, 2010499.
[4] P. Albertus, S. Babinec, S. Litzelman, A. Newman, *Nat. Energy* **2018**, *3*, 16.
[5] Y. Shao, F. Ding, J. Xiao, J. Zhang, W. Xu, S. Park, J.-G. Zhang, Y. Wang, J. Liu, *Adv. Funct. Mater.* **2013**, *23*, 987.
[6] Y. Li, S. Guo, *Matter* **2021**, *4*, 1142.
[7] J. Lian, W. Guo, Y. Fu, *J. Am. Chem. Soc.* **2021**, *143*, 11063.
[8] X. Li, J. Zheng, X. Ren, M. H. Engelhard, W. Zhao, Q. Li, J.-G. Zhang, W. Xu, *Adv. Energy Mater.* **2018**, *8*, 1703022.
[9] Y. Ma, Z. Zhou, C. Li, L. Wang, Y. Wang, X. Cheng, P. Zuo, C. Du, H. Huo, Y. Gao, G. Yin, *Energy Stor. Mater.* **2018**, *11*, 197.
[10] S. Bai, Y. Sun, J. Yi, Y. He, Y. Qiao, H. Zhou, *Joule* **2018**, *2*, 2117.
[11] T.-S. Wang, X. Liu, X. Zhao, P. He, C.-W. Nan, L.-Z. Fan, *Adv. Funct. Mater.* **2020**, *30*, 30.
[12] N.-W. Li, Y.-X. Yin, C.-P. Yang, Y.-G. Guo, *Adv. Mater.* **1853**, *2016*, 28.
[13] Z. Yu, D. G. Mackanic, W. Michaels, M. Lee, A. Pei, D. Feng, Q. Zhang, Y. Tsao, C. V. Amanchukwu, X. Yan, H. Wang, S. Chen, K. Liu, J. Kang, J. Qin, Y. Cui, Z. Bao, *Joule* **2019**, *3*, 2761.
[14] D. Li, L. Chen, T. Wang, L.-Z. Fan, A. S. C. Appl, *Mater. Inter.* **2018**, *10*, 7069.
[15] Q. Wang, H. Wang, J. Wu, M. Zhou, W. Liu, H. Zhou, *Nano Energy* **2021**, *80*, 105516.
[16] S. Tang, W. Guo, Y. Fu, *Adv. Energy Mater.* **2021**, *11*, 2000802.
[17] Z. Wang, H. Xu, M. Xuan, G. Shao, *J. Mater. Chem. A* **2018**, *6*, 73.
[18] C. Zhao, G.-L. Xu, Z. Yu, L. Zhang, I. Hwang, Y.-X. Mo, Y. Ren, L. Cheng, C.-J. Sun, Y. Ren, X. Zuo, J.-T. Li, S.-G. Sun, K. Amine, T. Zhao, *Nat. Nanotech.* **2021**, *16*, 166.
[19] Z. Liu, Y. Du, P. Zhang, Z. Zhuang, D. Wang, *Matter* **2021**, *4*, 3161.
[20] Z. Liu, H. Song, Y. Zhao, R. He, J. Meng, Q. Yu, K. A. Owusu, C. Yu, D. Zhao, L. Zhou, *ACS Mater. Lett.* **2019**, *1*, 290.
[21] H. Ye, S. Xin, Y.-X. Yin, Y.-G. Guo, *Adv. Energy Mater.* **2017**, *7*, 1700530.
[22] J. Gu, Q. Zhu, Y. Shi, H. Chen, D. Zhang, Z. Du, S. Yang, *ACS Nano* **2020**, *14*, 891.

[23] P. Zhai, T. Wang, W. Yang, S. Cui, P. Zhang, A. Nie, Q. Zhang, Y. Gong, *Adv. Energy Mater.* **2019**, *9*, 1804019.

[24] Z. Yang, Y. Dang, P. Zhai, Y. Wei, Q. Chen, J. Zuo, X. Gu, Y. Yao, X. Wang, F. Zhao, J. Wang, S. Yang, P. Tang, Y. Gong, *Adv. Energy Mater.* **2022**, *12*, 2103368.

[25] Z. Zhuang, Y. Li, R. Yu, L. Xia, J. Yang, Z. Lang, J. Zhu, J. Huang, J. Wang, Y. Wang, L. Fan, J. Wu, Y. Zhao, D. Wang, Y. Li, *Nat. Cat.* **2022**, *5*, 300.

[26] J. N. Chazalviel, *Phys. Rev. A* **1990**, *42*, 7355.

[27] F. Zhang, X. Liu, M. Yang, X. Cao, X. Huang, Y. Tian, F. Zhang, H. Li, *Nano Energy* **2020**, *69*, 104443.

[28] Q. Yu, J. Lv, Z. Liu, M. Xu, W. Yang, K. A. Owusu, L. Mai, D. Zhao, L. Zhou, *Sci. Bull.* **2019**, *64*, 1617.

[29] D. Liu, J.-H. Lei, L.-P. Guo, D. Qu, Y. Li, B.-L. Su, *Carbon* **2012**, *50*, 476.

[30] G.-H. Wang, Z. Cao, D. Gu, N. Pfänder, A.-C. Swertz, B. Spliethoff, H.-J. Bongard, C. Weidenthaler, W. Schmidt, R. Rinaldi, F. Schüth, *Angew. Chem. Int. Ed.* **2016**, *55*, 8850.

[31] P. Veerakumar, I. Panneer Muthuselvam, P. Thanasekaran, K.-C. Lin, *Inorg. Chem. Front.* **2018**, *5*, 354.

[32] J. Xiao, Q. Li, Y. Bi, M. Cai, B. Dunn, T. Glossmann, J. Liu, T. Osaka, R. Sugiura, B. Wu, J. Yang, J.-G. Zhang, M. S. Whittingham, *Nat. Energy* **2020**, *5*, 561.

[33] X. Chen, X.-R. Chen, T.-Z. Hou, B.-Q. Li, X.-B. Cheng, R. Zhang, Q. Zhang, *Sci. Adv.* **2019**, *5*, eaau7728.

[34] C. Yu, Y. Du, R. He, Y. Ma, Z. Liu, X. Li, W. Luo, L. Zhou, L. Mai, *ACS Appl. Energy Mater.* **2021**, *4*, 3905.

[35] K. Yan, Z. Lu, H.-W. Lee, F. Xiong, P.-C. Hsu, Y. Li, J. Zhao, S. Chu, Y. Cui, *Nat. Energy* **2016**, *1*, 16010.

[36] S. Liu, Z. Lin, F. Xiao, J. Zhang, D. Wang, X. Chen, Y. Zhao, J. Xu, *Chem. Eng. J.* **2020**, *389*, 124377.

[37] S. Chen, T. Liu, J. Ge, J. Hong, Y. Wang, *ACS Appl. Energy Mater.* **2022**, *5*, 539.